Spatio-angular transfer functions for fluorescence microscopes I. Basic theory

TALON CHANDLER,[1,*] AUTHOR ORDER TBD,[2,*] AND PATRICK LA RIVIÈRE [1]

[1] *University of Chicago, Department of Radiology, Chicago, Illinois 60637, USA*
[2] *Publications Department, The Optical Society, 2010 Massachusetts Avenue NW, Washington, DC 20036, USA*
[3] *Currently with the Department of Electronic Journals, The Optical Society, 2010 Massachusetts Avenue NW, Washington, DC 20036, USA*
[*] *talonchandler@talonchandler.com*

Abstract: We introduce the basic elements of a complete spatio-angular theory of fluorescence microscopes. We start by analyzing a single-view fluorescence microscope imaging an ensemble of in-focus dipole absorber/emitters using electromagnetic optics and the paraxial approximation. Next, we define the spatio-angular transfer function and show that fluorescence microscopes have an angular band limit. Finally, we discuss the implications of our analysis on quantitative fluorescence microscopy studies.

1. Introduction

Fluorescence microscopes are ubiquitous tools in biology [XXX], materials science [XXX], and metrology [XXX] for measuring the concentration of fluorophores throughout a sample. While an unprocessed fluorescence micrograph reports the approximate concentration of fluorophores throughout a sample, diffraction-limited microscopes image a spatially blurred version of the true fluorophore distribution. Therefore, microscopists who are interested in accurate measurements will perform a computational restoration to recover some of the information lost during the imaging process.

Restoration techniques attempt to recover the true distribution of fluorophores using the measured data and a model of the imaging process. The model of the imaging process can be obtained theoretically (by mathematically modeling the instrument under idealized conditions), experimentally (by measuring the microscope's response to a known input), or by a combination of theory and experiment (by measuring parameters of an instrument model). In all cases, the accuracy of the restored image is limited by the accuracy of the imaging model.

Most theoretical fluorescence microscopy imaging models make simplifying approximations. A common (often unstated) pair of approximations is to (1) treat fluorophores as monopole absorber/emitters and (2) treat light propagation under the scalar approximation. In this work we will analyze fluorescence microscopes without these approximations and find the conditions under which these approximations are valid.

Using an experimentally determined model is an effective way to find an accurate model without understanding all of the physical details of the imaging system, but these approaches require a known input that can completely characterize the imaging system. Sub-diffraction beads are commonly used as a known input for measuring the response of a microscope, but we argue that sub-diffraction beads are not enough to completely characterize the response of a microscope to all fluorescent samples. Beads can only characterize the response of the microscope to an angularly uniform distribution of fluorophores, and we will show that all microscopes have an orientation-dependent response. A complete characterization requires a test sample with at least three known orientation distributions.

The single-molecule localization microscopy (SMLM) community has pioneered the use of rigorous electromagnetic models of single fluorescence microscopes [1, 2]. When only one

fluorophore is emitting at a time, the measured intensity pattern is strongly dependent on the orientation of the emitting molecule. Backlund and Lew [3] have shown that ignoring the orientation of fluorophores can lead to biased estimates of their position, so the most accurate SMLM experiments must jointly estimate the position and orientation of the molecule. These joint estimates usually use a set of precomputed intensity patterns and a maximum-likelihood algorithm to estimate the orientation and position of each molecule. These methods have led to some of the most accurate position estimates of single molecules.

Meanwhile, most fluorescence microscopists image ensembles of fluorophores. Although many groups have used polarizers to probe the orientation of ensembles of fluorophores [4] [Forkey], to our knowledge no work has been done on the response of fluorescence microscopes to ensembles of oriented fluorophores. Furthermore, current restoration techniques in polarized light microscopy are lacking because they rely on simple pixel-wise arithmetic and do not model the propagation of light through the microscope.

In this work we model ensembles of in-focus dipole absorber/emitters using electromagnetic optics and the paraxial approximation. This marks a first step towards a complete three-dimensional non-paraxial theory of fluorescence microscopes. In section 2 we model the excitation and detection processes of dipoles. We define the most important quantity in this work, the spatio-angular transfer function, and we use it to show that fluorescence microscopes have an angular band limit. In section 3 we perform simulations and compare our model to traditional scalar models. In section 4 we discuss the implications of our work for fluorescence microscopy and lay out a path towards a complete spatio-angular theory of fluorescence microscopy.

2. Theory

2.1. Spherical harmonics

$$y_l^m(\vartheta,\varphi) = \begin{cases} \sqrt{2}K_l^m \cos(m\varphi)P_l^m(\cos\vartheta), & m > 0 \\ K_l^0 P_l^0(\cos\vartheta), & m = 0 \\ \sqrt{2}K_l^m \sin(-m\varphi)P_l^{-m}(\cos\vartheta), & m < 0 \end{cases} \tag{1}$$

where

$$K_l^m = \sqrt{\frac{(2l+1)}{4\pi}\frac{(l-|m|)!}{(l+|m|)!}}, \tag{2}$$

and $P_l^m(x)$ are the associated Legendre polynomials. The $l = 0, 1, 2$ spherical harmonics are given by

$$\begin{gathered} y_0^0(\vartheta,\varphi) = \sqrt{\frac{1}{4\pi}}, \\ y_1^{-1}(\vartheta,\varphi) = \sqrt{\frac{3}{4\pi}}\sin\varphi\sin\vartheta, \qquad y_1^0(\vartheta,\varphi) = \sqrt{\frac{3}{4\pi}}\cos\vartheta, \qquad y_1^1(\vartheta,\varphi) = \sqrt{\frac{3}{4\pi}}\cos\varphi\sin\vartheta, \\ y_2^{-2}(\vartheta,\varphi) = \sqrt{\frac{15}{4\pi}}\sin\varphi\cos\varphi\sin^2\vartheta, \qquad y_2^{-1}(\vartheta,\varphi) = \sqrt{\frac{15}{4\pi}}\sin\varphi\sin\vartheta\cos\vartheta, \\ y_2^0(\vartheta,\varphi) = \sqrt{\frac{5}{16\pi}}(3\cos^2\vartheta - 1), \\ y_2^1(\vartheta,\varphi) = \sqrt{\frac{15}{4\pi}}\cos\varphi\sin\vartheta\cos\vartheta, \qquad y_2^2(\vartheta,\varphi) = \sqrt{\frac{15}{4\pi}}(\cos^2\varphi - \sin^2\varphi)\sin^2\vartheta. \end{gathered} \tag{3}$$

2.2. Excitation model

In this section we will calculate the excitation kernel for epi-illumination microscopes—the relative probability of exciting a molecule with a known orientation. Our approach is similar to previous work [5, 6], but here we consider unpolarized illumination and restrict ourselves to the paraxial approximation.

We consider a single molecule with a fixed absorption dipole moment $\hat{\mathbf{s}}_o$ that we express in spherical coordinates [see Fig. 1(a)] as

$$\hat{\mathbf{s}}_o = \cos\varphi \sin\vartheta \hat{\mathbf{x}} + \sin\varphi \sin\vartheta \hat{\mathbf{y}} + \cos\vartheta \hat{\mathbf{z}}. \tag{4}$$

We can rewrite Eq. 4 in terms of spherical harmonic functions (see Section 2.1) as

$$\hat{\mathbf{s}}_o = \sqrt{\frac{3}{4\pi}} \left[y_1^1(\vartheta, \varphi)\, \hat{\mathbf{x}} + y_1^{-1}(\vartheta, \varphi)\, \hat{\mathbf{y}} + y_1^0(\vartheta, \varphi)\, \hat{\mathbf{z}} \right]. \tag{5}$$

We place the molecule in the focal plane of an aplanatic and polarization-preserving objective lens with its optical axis aligned with the $\hat{\mathbf{z}}$ axis. Next, we place a spatially incoherent, spatially uniform, unpolarized thermal light source (or its image) in the back aperture of the objective lens to illuminate the focal plane. In this geometry each point in the back focal plane generates a plane wave that illuminates the sample.

To model the unpolarized light source we will use polarized ray tracing [cite Torok] to find the response for a single polarized ray, then integrate over the rays and polarizations to find the complete response. First, we model the electric field at every point on the back focal plane as

$$\mathbf{E}_{\text{bfp}}(\phi_{\text{pol}}) \propto \cos\phi_{\text{pol}} \hat{\mathbf{x}} + \sin\phi_{\text{pol}} \hat{\mathbf{y}}, \tag{6}$$

where ϕ_{pol} is the polarization orientation and $\{\hat{\mathbf{x}}, \hat{\mathbf{y}}\}$ are transverse Cartesian basis vectors. Notice that Eq. 6 describes the incoherent electric fields at every point in the back focal plane, it does not describe a coherent plane wave. Immediately after the lens the electric field is

$$\mathbf{E}_{\text{ff}}(\theta, \phi, \phi_{\text{pol}}) \propto \left\{ [\mathbf{E}_{\text{bfp}}(\phi_{\text{pol}}) \cdot \hat{\boldsymbol{\phi}}]\, \hat{\boldsymbol{\phi}} + [\mathbf{E}_{\text{bfp}}(\phi_{\text{pol}}) \cdot \hat{\boldsymbol{\rho}}]\, \hat{\boldsymbol{\theta}} \right\} \sqrt{\cos\theta}, \tag{7}$$

where $\{\theta, \phi\}$ are spherical coordinates, $\{\hat{\boldsymbol{\rho}}, \hat{\boldsymbol{\phi}}\}$ are cylindrical basis vectors, and $\{\hat{\boldsymbol{\theta}}, \hat{\boldsymbol{\phi}}\}$ are spherical basis vectors defined in Figure 1(a) and related by

$$\hat{\boldsymbol{\rho}} = \cos\phi \hat{\mathbf{x}} + \sin\phi \hat{\mathbf{y}}, \tag{8}$$

$$\hat{\boldsymbol{\phi}} = -\sin\phi \hat{\mathbf{x}} + \cos\phi \hat{\mathbf{y}}, \tag{9}$$

$$\hat{\boldsymbol{\theta}} = \cos\phi \cos\theta \hat{\mathbf{x}} + \sin\phi \cos\theta \hat{\mathbf{y}} - \sin\theta \hat{\mathbf{z}}. \tag{10}$$

In Eq. 7 the $[\mathbf{E}_{\text{bfp}}(\phi_{\text{pol}}) \cdot \hat{\boldsymbol{\phi}}]\, \hat{\boldsymbol{\phi}}$ term models s-polarized fields, the $[\mathbf{E}_{\text{bfp}}(\phi_{\text{pol}}) \cdot \hat{\boldsymbol{\rho}}]\, \hat{\boldsymbol{\theta}}$ term models the rotation of p-polarized fields, and the $\sqrt{\cos\theta}$ term models the apodization of an aplanatic lens. After plugging Eq. 6 and Eqs. 8–10 into Eq. 7 and applying the paraxial approximation, the electric field immediately after the lens is given by

$$\mathbf{E}_{\text{ff}}^{(p)}(\theta, \phi, \phi_{\text{pol}}) \propto \cos\phi_{\text{pol}} \hat{\mathbf{x}} + \sin\phi_{\text{pol}} \hat{\mathbf{y}} - \theta \cos(\phi - \phi_{\text{pol}}) \hat{\mathbf{z}}. \tag{11}$$

To calculate the probability that a dipole oriented along $\hat{\mathbf{s}}_o$ is excited by a ray with electric field $\mathbf{E}$ we need to evaluate $|\mathbf{E} \cdot \hat{\mathbf{s}}_o|^2$. Evaluating this expression for each ray would be cumbersome if we used Eqs. 4 and 11 because we would need to simplify a large number of trigonometric functions. Instead, we use Eqs. 5 and 11 and the real Gaunt coefficients [XXXciteXXX] to find

the products of spherical harmonics. We find that

$$|\mathbf{E}_{\mathrm{ff}}^{(p)}(\theta,\phi,\phi_{\mathrm{pol}})\cdot\hat{\mathbf{s}}_o|^2 \propto \left[1+\theta^2\cos^2(\phi-\phi_{\mathrm{pol}})\right] y_0^0(\hat{\mathbf{s}}_o) + \frac{1}{\sqrt{5}}\left[-1+2\theta^2\cos^2(\phi-\phi_{\mathrm{pol}})\right] y_2^0(\hat{\mathbf{s}}_o) + \frac{\sqrt{15}}{10}\theta\sin\phi_{\mathrm{pol}}\cos(\phi-\phi_{\mathrm{pol}}) y_2^{-1}(\hat{\mathbf{s}}_o) + \frac{\sqrt{15}}{10}\theta\cos\phi_{\mathrm{pol}}\cos(\phi-\phi_{\mathrm{pol}}) y_2^{1}(\hat{\mathbf{s}}_o) - \frac{\sqrt{15}}{20}\sin(2\phi_{\mathrm{pol}}) y_2^{-2}(\hat{\mathbf{s}}_o) - \frac{\sqrt{15}}{20}\cos(2\phi_{\mathrm{pol}}) y_2^{2}(\hat{\mathbf{s}}_o). \tag{12}$$

To calculate the complete excitation model we need to integrate Eq. 12 over all polarization orientations and rays

$$h_{\mathrm{exc}}(\hat{\mathbf{s}}_o) \propto \int_0^{\alpha} \theta d\theta \int_0^{2\pi} d\phi \int_0^{2\pi} d\phi_{\mathrm{pol}}\, |\mathbf{E}_{\mathrm{ff}}^{(p)}\cdot\hat{\mathbf{s}}_o|^2. \tag{13}$$

After plugging Eq. 12 into Eq. 13 and evaluating the integrals, all but two terms disappear and the orientation-dependent excitation model is given by

$$h_{\mathrm{exc}}(\hat{\mathbf{s}}_o) \propto \left[1+\frac{\alpha^2}{4}\right] y_0^0(\hat{\mathbf{s}}_o) + \frac{1}{\sqrt{5}}\left[-1+\frac{\alpha^2}{2}\right] y_2^0(\hat{\mathbf{s}}_o). \tag{14}$$

We note that the excitation model depends on the orientation of the molecule, but it does not depend on the position of the molecule in the focal plane. This is a direct consequence of our illumination geometry—we have placed incoherent light sources in the back focal plane of the objective so each point in the focal plane within the field of view is illuminated equally.

2.3. Detection model

In this section we will calculate the detection kernel of an epi-detection microscope—the irradiance on the detector due to single molecule at a known position with known orientation. Our approach is similar to [1, 7, 8], but here we restrict ourselves to the paraxial approximation.

We consider a single dipole emitter at the origin with a fixed dipole emission moment oriented along $\hat{\mathbf{s}}_o$—parallel to the excitation moment. The electric field at a position $\mathbf{r}$ far from the dipole is given by

$$\mathbf{E}_{\mathrm{ff}}(\mathbf{r},\hat{\mathbf{s}}_o) \propto \hat{\mathbf{r}}\times\hat{\mathbf{s}}_o\times\hat{\mathbf{r}}. \tag{15}$$

If we place the molecule in the focal plane of an aplanatic and polarization-preserving objective lens with its optical axis aligned with the $\hat{\mathbf{z}}$ axis (or reuse the illumination objective), then the electric field in the back focal plane of the lens is given by

$$\mathbf{E}_{\mathrm{bfp}}(\mathbf{r}_b,\hat{\mathbf{s}}_o) \propto \left\{[\mathbf{E}_{\mathrm{ff}}(\mathbf{r},\hat{\mathbf{s}}_o)\cdot\hat{\boldsymbol{\phi}}]\,\hat{\boldsymbol{\phi}} + [\mathbf{E}_{\mathrm{ff}}(\mathbf{r},\hat{\mathbf{s}}_o)\cdot\hat{\boldsymbol{\theta}}]\,\hat{\boldsymbol{\rho}}\right\}\sqrt{1/\cos\theta}\,\Pi\left(\frac{r_b}{\sin\alpha}\right). \tag{16}$$

where the first term accounts for s-polarized fields, the second term accounts for p-polarized fields, $\sqrt{1/\cos\theta}$ is the apodization factor for an aplanatic lens, and

$$\Pi\left(\frac{r_b}{\sin\alpha}\right) = \begin{cases} 1 & \text{if} \quad r_b < \sin^{-1}\alpha, \\ 0 & \text{else,} \end{cases} \tag{17}$$

is the aperture stop. After expanding the dot products, applying the paraxial approximation, and writing the dipole orientation $\hat{\mathbf{s}}_o$ in terms of spherical harmonic functions, we find that the electric field in the back focal plane is given by

$$\mathbf{E}_{\mathrm{bfp}}^{(p)}(\mathbf{r}_b,\hat{\mathbf{s}}_o) \propto \left\{\left[y_1^1(\hat{\mathbf{s}}_o) - r_b\cos\phi_b y_1^0(\hat{\mathbf{s}}_o)\right]\hat{\mathbf{x}} + \left[y_1^{-1}(\hat{\mathbf{s}}_o) - r_b\sin\phi_b y_1^0(\hat{\mathbf{s}}_o)\right]\hat{\mathbf{y}}\right\}\Pi\left(\frac{r_b}{\alpha}\right). \tag{18}$$

We note that Eq. 18 is identical to previously derived models [Piestun, Backer] except here we have used the paraxial approximation and used spherical harmonic functions.

Next we place a tube lens one focal length from the back focal plane and a detector (see Figure XX)). Under the paraxial approximation we can find the electric field in the detector plane by taking the Fourier transform of the field in the back focal plane [Goodman]

$$\mathbf{E}^{(p)}_{\text{det}}(\mathbf{r}_d, \hat{\mathbf{s}}_o) = \int_{\mathbb{R}^2} d\mathbf{r}_b \mathbf{E}^{(p)}_{\text{bfp}}(\mathbf{r}_b) \exp\left[ik\, \mathbf{r}_b \cdot \mathbf{r}_d\right]. \tag{19}$$

To evaluate the integral we rewrite it in polar coordinates

$$\mathbf{E}^{(p)}_{\text{det}}(\mathbf{r}_d, \hat{\mathbf{s}}_o) = \int_0^{\alpha} r_b dr_b \int_0^{2\pi} d\phi_b\, \mathbf{E}^{(p)}_{\text{bfp}}(r_b, \phi_b) \exp\left[ikr_b r_d \cos(\phi_b - \phi_d)\right], \tag{20}$$

substitute Eq. 18, and apply the following identities

$$\int_0^{2\pi} d\phi_b \begin{Bmatrix} \sin(n\phi_b) \\ \cos(n\phi_b) \end{Bmatrix} \exp\left[ikr_b r_d \cos(\phi_b - \phi_d)\right] = 2\pi i^n \begin{Bmatrix} \sin(n\phi'_o) \\ \cos(n\phi'_o) \end{Bmatrix} J_n(kr_b r_d), \tag{21}$$

$$\int_0^{\alpha} dr_b (r_b)^{n+1} J_n(kr_b r_d) = \alpha^{n+1} \left[\frac{J_{n+1}(k\alpha r_d)}{kr_d}\right], \tag{22}$$

to find that

$$\begin{aligned} \mathbf{E}^{(p)}_{\text{det}}(\mathbf{r}_d, \hat{\mathbf{s}}_o) \propto &\left[\frac{J_1(k\alpha r_d)}{k\alpha r_d} y_1^1(\hat{\mathbf{s}}_o) - i\alpha \frac{J_2(k\alpha r_d)}{k\alpha r_d} \cos\phi_d y_1^0(\hat{\mathbf{s}}_o)\right] \hat{\mathbf{x}} + \\ &\left[\frac{J_1(k\alpha r_d)}{k\alpha r_d} y_1^{-1}(\hat{\mathbf{s}}_o) - i\alpha \frac{J_2(k\alpha r_d)}{k\alpha r_d} \sin\phi_d y_1^0(\hat{\mathbf{s}}_o)\right] \hat{\mathbf{y}}. \end{aligned} \tag{23}$$

We can find the irradiance on the detector by taking the modulus squared of the electric field

$$h_{\text{det}}(\mathbf{r}_d, \hat{\mathbf{s}}_o) \propto |\mathbf{E}^{(p)}_{\text{det}}(\mathbf{r}_d, \hat{\mathbf{s}}_o)|^2. \tag{24}$$

We use the real Gaunt coefficients to find that

$$h_{\text{det}}(\mathbf{r}_d, \hat{\mathbf{s}}_o) \propto \left[a_1(r_d) + \frac{\alpha^2}{4} a_2(r_d)\right] y_0^0(\hat{\mathbf{s}}_o) + \frac{1}{\sqrt{5}} \left[-a_1(r_d) + \frac{\alpha^2}{2} a_2(r_d)\right] y_2^0(\hat{\mathbf{s}}_o), \tag{25}$$

where we have defined

$$a_n(r_d) \equiv \frac{n}{\pi} \left[\frac{J_n(k\alpha r_d)}{k\alpha r_d}\right]^2. \tag{26}$$

In our analysis we have only considered a dipole radiator at the origin, but we can use the shift-invariance of $4f$ imaging systems to model dipole radiators at arbitrary positions in the focal plane. If we shift the dipole radiator to an in-focus position $\mathbf{r}_o$, then the irradiance pattern on the detector will be given by $h_{\text{det}}(\mathbf{r}_d - \mathbf{r}_o)$. We have also restricted our analysis to an imaging system with unit magnification, but an imaging system with an arbitrary magnification can be modeled as a system with unit magnification using a change of variables (see [9] section 7.2.7).

Finally, we note the similarities between Eqs. 14 and 25. If we integrate the detection kernel over the detector and use the identity $\int_{\mathbb{R}^2} d\mathbf{r}\, a_n(r) = 1$ for $n \in \mathbb{N}$, then we find that the excitation and detection kernels are related by

$$h_{\text{exc}}(\hat{\mathbf{s}}_o) = \int_{\mathbb{R}^2} d\mathbf{r} h_{\text{det}}(\mathbf{r}, \hat{\mathbf{s}}_o). \tag{27}$$

2.4. Complete forward model

In the last two section we have found closed-form expressions for the excitation kernel $h_{\text{exc}}(\hat{\mathbf{s}}_o)$ and the detection kernel $h_{\text{det}}(\mathbf{r}_d - \mathbf{r}_o, \hat{\mathbf{s}}_o)$. The complete kernel of the microscope is the product of the excitation and detection kernels

$$h(\mathbf{r}_d - \mathbf{r}_o, \hat{\mathbf{s}}_o) = h_{\text{exc}}(\hat{\mathbf{s}}_o) h_{\text{det}}(\mathbf{r}_d - \mathbf{r}_o, \hat{\mathbf{s}}_o). \tag{28}$$

Eq. 28 gives the irradiance at position $\mathbf{r}_d$ on the detector created by a single dipole at position $\mathbf{r}_o$ with dipole oriented along $\hat{\mathbf{s}}_o$.

Up to this point we have only modeled the imaging system's response to single fluorescent molecules. We would like to model samples that contain ensembles of fluorescent molecules with many fluorescent molecules, so we introduce the *spatio-angular density* to describe arbitrary distributions of fluorescent dipoles. We define the spatio-angular density $f(\mathbf{r}_o, \hat{\mathbf{s}}_o)$ as the number of fluorescent molecules at position $\mathbf{r}_o$ per unit volume oriented along $\hat{\mathbf{s}}_o$ per unit solid angle. Figure TODO illustrates several simple spatio-angular densities to clarify our definition.

The detector irradiance $g(\mathbf{r}_d)$ created by an arbitrary spatio-angular density $f(\mathbf{r}_o, \hat{\mathbf{s}}_o)$ can be found by multiplying the spatio-angular density by the kernel and integrating over all positions $\mathbf{r}_o$ and orientations $\hat{\mathbf{s}}_o$

$$g(\mathbf{r}_d) = \int_{\mathbb{S}^2} d\hat{\mathbf{s}}_o \int_{\mathbb{R}^2} d\mathbf{r}_o \, h(\mathbf{r}_d - \mathbf{r}_o, \hat{\mathbf{s}}_o) f(\mathbf{r}_o, \hat{\mathbf{s}}_o). \tag{29}$$

2.5. Spatio-angular transfer function

As written Eq. 29 is an extremely expensive integral to compute—to find the irradiance at a single point on the detector we need to evaluate the spatio-angular density and the kernel at every point in $\mathbb{S}^2 \times \mathbb{R}^2$. To simplify the integral, we expand the object and the kernel onto complex exponentials and spherical harmonics using

$$F_l^m(\boldsymbol{\nu}) \equiv \int_{\mathbb{S}^2} d\hat{\mathbf{s}}_o y_l^m(\hat{\mathbf{s}}_o) \int_{\mathbb{R}^2} d\mathbf{r}_o \exp\left[i2\pi \mathbf{r}_o \cdot \boldsymbol{\nu}\right] f(\mathbf{r}_o, \hat{\mathbf{s}}_o), \tag{30}$$

$$H_l^m(\boldsymbol{\nu}) \equiv \int_{\mathbb{S}^2} d\hat{\mathbf{s}}_o y_l^m(\hat{\mathbf{s}}_o) \int_{\mathbb{R}^2} d\mathbf{r}_o \exp\left[i2\pi \mathbf{r}_o \cdot \boldsymbol{\nu}\right] h(\mathbf{r}_o, \hat{\mathbf{s}}_o). \tag{31}$$

We also expand the detector irradiance onto spatial harmonics using the Fourier transform

$$G(\boldsymbol{\nu}) \equiv \int_{\mathbb{R}^2} d\mathbf{r}_d \exp\left[i2\pi \mathbf{r}_d \cdot \boldsymbol{\nu}\right] g(\mathbf{r}_d). \tag{32}$$

Given these definitions, we can rewrite Eq. 29 in the frequency domain as

$$G(\boldsymbol{\nu}) = \sum_{l=0}^{\infty} \sum_{m=-l}^{l} H_l^m(\boldsymbol{\nu}) F_l^m(\boldsymbol{\nu}). \tag{33}$$

In Appendix A we calculate the spatio-angular transfer function as

$$\begin{aligned} H_l^m(\boldsymbol{\nu}) = \frac{1}{C} \Bigg\{ & \left[\left(1 + \frac{\alpha^2}{8}\right) A_1(\nu) + \left(\frac{\alpha^2}{8} + \frac{3\alpha^4}{32}\right) A_2(\nu) \right] \delta_{l0}\delta_{m0} + \\ & \frac{2\sqrt{5}}{7} \left[\left(-1 + \frac{\alpha^2}{16}\right) A_1(\nu) + \left(\frac{\alpha^2}{16} + \frac{3\alpha^4}{16}\right) A_2(\nu) \right] \delta_{l2}\delta_{m0} \\ & \frac{1}{7} \left[\left(1 - \frac{\alpha^2}{2}\right) A_1(\nu) + \left(-\frac{\alpha^2}{2} + \frac{\alpha^4}{4}\right) A_2(\nu) \right] \delta_{l4}\delta_{m0} \Bigg\}, \end{aligned} \tag{34}$$

where

$$A_1(\nu) = \frac{2}{\pi}\left\{\cos^{-1}\left(\frac{\nu}{2\nu_o}\right) - \frac{\nu}{2\nu_o}\sqrt{1-\left(\frac{\nu}{2\nu_o}\right)^2}\right\}\Pi\left(\frac{\nu}{2\nu_o}\right), \tag{35}$$

$$A_2(\nu) = \frac{2}{\pi}\left\{\cos^{-1}\left(\frac{\nu}{2\nu_o}\right) - \left[3-2\left(\frac{\nu}{2\nu_o}\right)^2\right]\frac{\nu}{2\nu_o}\sqrt{1-\left(\frac{\nu}{2\nu_o}\right)^2}\right\}\Pi\left(\frac{\nu}{2\nu_o}\right), \tag{36}$$

and $C = 1 + \frac{\alpha^2}{4} + \frac{3\alpha^4}{32}$ is a normalization constant.

3. Results

4. Discussion and conclusion

References

1. A. S. Backer and W. E. Moerner, "Extending single-molecule microscopy using optical Fourier processing," J. Phys. Chem. B **118**, 8313–8329 (2014).
2. M. A. Lieb, J. M. Zavislan, and L. Novotny, "Single-molecule orientations determined by direct emission pattern imaging," J. Opt. Soc. Am. B **21**, 1210–1215 (2004).
3. M. P. Backlund, M. D. Lew, A. S. Backer, S. J. Sahl, and W. E. Moerner, "The role of molecular dipole orientation in single-molecule fluorescence microscopy and implications for super-resolution imaging," ChemPhysChem **15**, 587–599 (2014).
4. S. B. Mehta, M. McQuilken, P. J. La Rivière, P. Occhipinti, A. Verma, R. Oldenbourg, A. S. Gladfelter, and T. Tani, "Dissection of molecular assembly dynamics by tracking orientation and position of single molecules in live cells," Proc. Natl. Acad. Sci. U.S.A. **113**, E6352–E6361 (2016).
5. J. T. Fourkas, "Rapid determination of the three-dimensional orientation of single molecules," Opt. Lett. **26**, 211–213 (2001).
6. T. Chandler, S. Mehta, H. Shroff, R. Oldenbourg, and P. J. La Rivière, "Single-fluorophore orientation determination with multiview polarized illumination: modeling and microscope design," Opt. Express **25**, 31309–31325 (2017).
7. L. Novotny and B. Hecht, *Principles of Nano-Optics* (Cambridge University Press, 2006).
8. A. Agrawal, S. Quirin, G. Grover, and R. Piestun, "Limits of 3D dipole localization and orientation estimation for single-molecule imaging: towards Green's tensor engineering," Opt. Express **20**, 26667–26680 (2012).
9. H. Barrett and K. Myers, *Foundations of image science*, Wiley series in pure and applied optics (Wiley-Interscience, 2004).
10. J. Goodman, *Introduction to Fourier Optics* (McGraw-Hill, 1996), 2nd ed.
11. J. Mertz, *Introduction to Optical Microscopy* (W. H. Freeman, 2009).
12. A. Poularikas, *Handbook of Formulas and Tables for Signal Processing*, Electrical Engineering Handbook (CRC-Press, 1998).

A. Evaluating the spatio-angular transfer function

In this appendix we will evaluate

$$H_l^m(\boldsymbol{\nu}) \propto \int_{\mathbb{S}^2} d\hat{\mathbf{s}}_o\, y_l^m(\hat{\mathbf{s}}_o) \int_{\mathbb{R}^2} d\mathbf{r}_o \exp\left[i2\pi\mathbf{r}_o\cdot\boldsymbol{\nu}\right] h(\mathbf{r}_o,\hat{\mathbf{s}}_o), \tag{37}$$

where

$$h(\mathbf{r}_d-\mathbf{r}_o,\hat{\mathbf{s}}_o) \propto h_{\text{exc}}(\hat{\mathbf{s}}_o)h_{\text{det}}(\mathbf{r}_d-\mathbf{r}_o,\hat{\mathbf{s}}_o), \tag{38}$$

$$h_{\text{exc}}(\hat{\mathbf{s}}_o) \propto \left[1+\frac{\alpha^2}{4}\right]y_0^0(\hat{\mathbf{s}}_o) + \frac{1}{\sqrt{5}}\left[-1+\frac{\alpha^2}{2}\right]y_2^0(\hat{\mathbf{s}}_o), \tag{39}$$

$$h_{\text{det}}(\mathbf{r}_d,\hat{\mathbf{s}}_o) \propto \left[a_1(r_d)+\frac{\alpha^2}{4}a_2(r_d)\right]y_0^0(\hat{\mathbf{s}}_o) + \frac{1}{\sqrt{5}}\left[-a_1(r_d)+\frac{\alpha^2}{2}a_2(r_d)\right]y_2^0(\hat{\mathbf{s}}_o), \tag{40}$$

and

$$a_n(r_d) \equiv \frac{n}{\pi}\left[\frac{J_n(k\alpha r_d)}{k\alpha r_d}\right]^2. \tag{41}$$

First we plug Eq. 38 into Eq. 37 and move the excitation kernel out of the spatial integral

$$H_l^m(\boldsymbol{\nu}) \propto \int_{\mathbb{S}^2} d\hat{\mathbf{s}}_o y_l^m(\hat{\mathbf{s}}_o) h_{\text{exc}}(\hat{\mathbf{s}}_o) \int_{\mathbb{R}^2} d\mathbf{r}_o \exp\left[i2\pi\mathbf{r}_o \cdot \boldsymbol{\nu}\right] h_{\text{det}}(\mathbf{r}_d, \hat{\mathbf{s}}_o). \tag{42}$$

The spatial integral requires us to evaluate the two-dimensional Fourier transform of $a_1(r_o)$ and $a_2(r_o)$. We will define

$$A_n(\nu) \equiv \mathcal{F}_2\{a_n(r_o)\} = \int_{\mathbb{R}^2} d\mathbf{r}_o \exp\left[i2\pi\mathbf{r}_o \cdot \boldsymbol{\nu}\right] a_n(r_d), \tag{43}$$

and evaluate $A_1(\nu)$ and $A_2(\nu)$ later. After substituting 43 into Eq. 42 we find

$$\begin{aligned} H_l^m(\boldsymbol{\nu}) \propto \int_{\mathbb{S}^2} d\hat{\mathbf{s}}_o y_l^m(\hat{\mathbf{s}}_o) \Bigg\{ &\left[1 + \frac{\alpha^2}{4}\right] y_0^0(\hat{\mathbf{s}}_o) + \frac{1}{\sqrt{5}}\left[-1 + \frac{\alpha^2}{2}\right] y_2^0(\hat{\mathbf{s}}_o)\Bigg\} + \\ &\Bigg\{\left[A_1(\nu) + \frac{\alpha^2}{4}A_2(\nu)\right] y_0^0(\hat{\mathbf{s}}_o) + \frac{1}{\sqrt{5}}\left[-A_1(\nu) + \frac{\alpha^2}{2}A_2(\nu)\right] y_2^0(\hat{\mathbf{s}}_o)\Bigg\}. \end{aligned} \tag{44}$$

After expanding the products of spherical harmonics

$$\begin{aligned} H_l^m(\boldsymbol{\nu}) \propto \int_{\mathbb{S}^2} d\hat{\mathbf{s}}_o y_l^m(\hat{\mathbf{s}}_o) \Bigg\{ &\left[\frac{3}{5}A_1(\nu) + \frac{3\alpha^2}{40}[A_1(\nu) + A_2(\nu)] + \frac{9\alpha^4}{160}A_2(\nu)\right] y_0^0(\hat{\mathbf{s}}_o) + \\ &\frac{3\sqrt{5}}{280}\left[-16A_1(\nu) + \alpha^2[A_1(\nu) + A_2(\nu)] + 3\alpha^4 A_2(\nu)\right] y_2^0(\hat{\mathbf{s}}_o) \\ &\frac{3}{35}\left[\left(1 - \frac{\alpha^2}{2}\right)A_1(\nu) + \left(-\frac{\alpha^2}{2} + \frac{\alpha^4}{4}\right)A_2(\nu)\right] y_4^0(\hat{\mathbf{s}}_o)\Bigg\}, \end{aligned} \tag{45}$$

$$\begin{aligned} H_l^m(\boldsymbol{\nu}) \propto \int_{\mathbb{S}^2} d\hat{\mathbf{s}}_o y_l^m(\hat{\mathbf{s}}_o) \Bigg\{ &\left[\left(1 + \frac{\alpha^2}{8}\right)A_1(\nu) + \left(\frac{\alpha^2}{8} + \frac{3\alpha^4}{32}\right)A_2(\nu)\right] y_0^0(\hat{\mathbf{s}}_o) + \\ &\frac{\sqrt{5}}{56}\left[(-16 + \alpha^2)A_1(\nu) + (\alpha^2 + 3\alpha^4)A_2(\nu)\right] y_2^0(\hat{\mathbf{s}}_o) \\ &\frac{1}{7}\left[\left(1 - \frac{\alpha^2}{2}\right)A_1(\nu) + \left(-\frac{\alpha^2}{2} + \frac{\alpha^4}{4}\right)A_2(\nu)\right] y_4^0(\hat{\mathbf{s}}_o)\Bigg\}. \end{aligned} \tag{46}$$

Next, we use the orthogonality of spherical harmonics to evaluate the angular integral

$$\begin{aligned} H_l^m(\boldsymbol{\nu}) = \frac{1}{C}\Bigg\{ &\left[\left(1 + \frac{\alpha^2}{8}\right)A_1(\nu) + \left(\frac{\alpha^2}{8} + \frac{3\alpha^4}{32}\right)A_2(\nu)\right]\delta_{l0}\delta_{m0} + \\ &\frac{2\sqrt{5}}{7}\left[\left(-1 + \frac{\alpha^2}{16}\right)A_1(\nu) + \left(\frac{\alpha^2}{16} + \frac{3\alpha^4}{16}\right)A_2(\nu)\right]\delta_{l2}\delta_{m0} \\ &\frac{1}{7}\left[\left(1 - \frac{\alpha^2}{2}\right)A_1(\nu) + \left(-\frac{\alpha^2}{2} + \frac{\alpha^4}{4}\right)A_2(\nu)\right]\delta_{l4}\delta_{m0}\Bigg\}, \end{aligned} \tag{47}$$

where $C = 1 + \frac{\alpha^2}{4} + \frac{3\alpha^4}{32}$ is a normalization constant.

Our final task is to calculate $A_1(\nu)$ and $A_2(\nu)$. $A_1(\nu)$ is a well-known result [10, 11], but we review the calculation to establish the tools we'll need to evaluate $A_2(\nu)$. We start by using the autocorrelation (Wiener-Khinchin) theorem to rewrite the Fourier transform as

$$A_1(\nu) = \frac{1}{\pi}\mathcal{F}_2\left\{\left[\frac{J_1(2\pi\nu_o r_o)}{2\pi\nu_o r_o}\right]^2\right\} = \frac{1}{\pi}\left[\mathcal{F}_2\left\{\frac{J_1(2\pi\nu_o r_o)}{2\pi\nu_o r_o}\right\} \star_2 \mathcal{F}_2\left\{\frac{J_1(2\pi\nu_o r_o)}{2\pi\nu_o r_o}\right\}\right] \tag{48}$$

where $\star_2$ denotes a two-dimensional autocorrelation. Next, we recognize that the Fourier transforms on the right hand side of Eq. 48 are rotationally symmetric so they can be rewritten as zero-order Hankel transforms

$$A_1(\nu) = \frac{1}{\pi}\left[\mathcal{H}_0\left\{\frac{J_1(2\pi\nu_o r_o)}{2\pi\nu_o r_o}\right\} \star_2 \mathcal{H}_0\left\{\frac{J_1(2\pi\nu_o r_o)}{2\pi\nu_o r_o}\right\}\right] \tag{49}$$

We can apply the Hankel transform identity [12]

$$\mathcal{H}_{n-1}\left\{\frac{J_n(2\pi\nu_o r_o)}{2\pi\nu_o r_o}\right\} = \frac{\nu^{n-1}}{\nu_o^n}\Pi\left(\frac{\nu}{\nu_o}\right), \tag{50}$$

to find that

$$A_1(\nu) = \frac{1}{\pi\nu_o^2}\left[\Pi\left(\frac{\nu}{\nu_o}\right) \star_2 \Pi\left(\frac{\nu}{\nu_o}\right)\right]. \tag{51}$$

We can use the geometric construction in Figure 1 to express the autocorrelation in terms of an integral over a region of overlap between two circles given by

$$A_1(\nu) = \frac{4}{\pi\nu_o^2}\left[\int_0^{\nu_o} \tau d\tau \int_0^{\cos^{-1}\left(\frac{\nu}{2\nu_o}\right)} d\phi_\tau - \int_0^{\nu/2} d\tau_x \int_0^{\tau_x \frac{2\nu_o}{\nu}\sqrt{1-\left(\frac{\nu}{2\nu_o}\right)^2}} d\tau_y\right]\Pi\left(\frac{\nu}{2\nu_o}\right), \tag{52}$$

$$A_1(\nu) = \frac{4}{\pi\nu_o^2}\left[\int_0^{\nu_o} \tau d\tau \cos^{-1}\left(\frac{\nu}{2\nu_o}\right) - \int_0^{\nu/2} d\tau_x \tau_x \frac{2\nu_o}{\nu}\sqrt{1-\left(\frac{\nu}{2\nu_o}\right)^2}\right]\Pi\left(\frac{\nu}{2\nu_o}\right), \tag{53}$$

$$A_1(\nu) = \frac{2}{\pi}\left\{\cos^{-1}\left(\frac{\nu}{2\nu_o}\right) - \frac{\nu}{2\nu_o}\sqrt{1-\left(\frac{\nu}{2\nu_o}\right)^2}\right\}\Pi\left(\frac{\nu}{2\nu_o}\right). \tag{54}$$

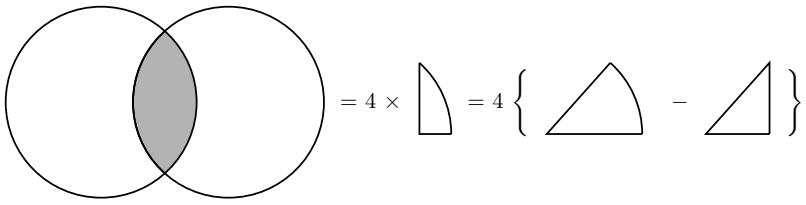

Fig. 1. Geometric construction for evaluating the autocorrelations. We need to integrate over the overlapping region of two circles with radius ν_o and distance ν between their centers. The region is given by four times the difference in area between a sector of angle $\arccos\left(\frac{\nu}{2\nu_o}\right)$ and a triangle with base $\nu/2$ and hypotenuse ν_o.

To evaluate $A_2(\nu)$ we could follow the same steps, but we will reach a dead end because there is no Hankel transform identity for $\mathcal{H}_{n-1}\left\{\frac{J_{n+1}(2\pi\nu_o r_o)}{2\pi\nu_o r_o}\right\}$. Instead, we rewrite $A_2(\nu)$ as

$$A_2(\nu) = \frac{2}{\pi}\mathcal{F}_2\left\{\left[\frac{J_2(2\pi\nu_o r_o)}{2\pi\nu_o r_o}\right]^2\right\} = \frac{2}{\pi}\left[\mathcal{F}_2\left\{\left[\frac{J_2(2\pi\nu_o r_o)}{2\pi\nu_o r_o}\cos\phi_\nu\right]^2\right\} + \mathcal{F}_2\left\{\left[\frac{J_2(2\pi\nu_o r_o)}{2\pi\nu_o r_o}\sin\phi_\nu\right]^2\right\}\right]. \tag{55}$$

Applying the autocorrelation theorem gives

$$A_2(\nu) = \frac{2}{\pi}\Bigg[\mathcal{F}_2\left\{\frac{J_2(2\pi\nu_o r_o)}{2\pi\nu_o r_o}\cos\phi_\nu\right\} \star_2 \mathcal{F}_2\left\{\frac{J_2(2\pi\nu_o r_o)}{2\pi\nu_o r_o}\cos\phi_\nu\right\} + \mathcal{F}_2\left\{\frac{J_2(2\pi\nu_o r_o)}{2\pi\nu_o r_o}\sin\phi_\nu\right\} \star_2 \mathcal{F}_2\left\{\frac{J_2(2\pi\nu_o r_o)}{2\pi\nu_o r_o}\sin\phi_\nu\right\}\Bigg]. \tag{56}$$

After converting the Fourier transforms to Hankel transforms with the identities

$$\mathcal{F}_2\left\{f(r)\cos(\phi)\right\} = -i\cos\phi_\nu \mathcal{H}_1\left\{f(r)\right\}, \tag{57}$$

$$\mathcal{F}_2\left\{f(r)\sin(\phi)\right\} = -i\sin\phi_\nu \mathcal{H}_1\left\{f(r)\right\}, \tag{58}$$

and evaluating the Hankel transforms with Eq. 50, we find that

$$A_2(\nu) = -\frac{2}{\pi\nu_o^4}\left\{\left[\nu_x\Pi\left(\frac{\nu}{\nu_o}\right) \star_2 \nu_x\Pi\left(\frac{\nu}{\nu_o}\right)\right] + \left[\nu_y\Pi\left(\frac{\nu}{\nu_o}\right) \star_2 \nu_y\Pi\left(\frac{\nu}{\nu_o}\right)\right]\right\}. \tag{59}$$

Eq. 59 contains two autocorrelations that require us to find the weighted overlap of two circles. Neither of these autocorrelations are rotationally symmetric, but their sum must be rotationally symmetric. With this symmetry in mind, we recognize that the first autocorrelation is largest for shifts along the x direction and smallest for shifts along the y direction with a smooth $\cos^2\phi_\nu$ weighting between the two extremes. The same is true for the second autocorrelations except the x and y axes are exchanged and there is a $\sin^2\phi_\nu$ weighting between the two extremes. Therefore, we can rewrite Eq. 59 as

$$A_2(\nu) = -\frac{2}{\pi\nu_o^4}\Bigg\{\left[\nu_x\Pi\left(\frac{\nu}{\nu_o}\right) \star_2^x \nu_x\Pi\left(\frac{\nu}{\nu_o}\right)\right]\cos^2\phi_\nu + \left[\nu_x\Pi\left(\frac{\nu}{\nu_o}\right) \star_2^y \nu_x\Pi\left(\frac{\nu}{\nu_o}\right)\right]\sin^2\phi_\nu + \left[\nu_y\Pi\left(\frac{\nu}{\nu_o}\right) \star_2^x \nu_y\Pi\left(\frac{\nu}{\nu_o}\right)\right]\cos^2\phi_\nu + \left[\nu_y\Pi\left(\frac{\nu}{\nu_o}\right) \star_2^y \nu_y\Pi\left(\frac{\nu}{\nu_o}\right)\right]\sin^2\phi_\nu\Bigg\}. \tag{60}$$

where $\star_2^x$ denotes a two-dimensional autocorrelation for shifts along the x direction. We can use the following pair of identities

$$\nu_x\Pi\left(\frac{\nu}{\nu_o}\right) \star_2^x \nu_x\Pi\left(\frac{\nu}{\nu_o}\right) = \nu_y\Pi\left(\frac{\nu}{\nu_o}\right) \star_2^y \nu_y\Pi\left(\frac{\nu}{\nu_o}\right), \tag{61}$$

$$\nu_x\Pi\left(\frac{\nu}{\nu_o}\right) \star_2^y \nu_x\Pi\left(\frac{\nu}{\nu_o}\right) = \nu_y\Pi\left(\frac{\nu}{\nu_o}\right) \star_2^x \nu_y\Pi\left(\frac{\nu}{\nu_o}\right), \tag{62}$$

to simplify Eq. 60 to

$$A_2(\nu) = -\frac{2}{\pi\nu_o^4}\left\{\left[\nu_x\Pi\left(\frac{\nu}{\nu_o}\right) \star_2^x \nu_x\Pi\left(\frac{\nu}{\nu_o}\right)\right] + \left[\nu_x\Pi\left(\frac{\nu}{\nu_o}\right) \star_2^y \nu_x\Pi\left(\frac{\nu}{\nu_o}\right)\right]\right\}. \tag{63}$$

First we evaluate the autocorrelation for shifts along the x axis

$$= -\frac{2}{\pi\nu_o^4}\left[\nu_x\Pi\left(\frac{\nu}{\nu_o}\right) \star_2^x \nu_x\Pi\left(\frac{\nu}{\nu_o}\right)\right] \tag{64}$$

$$= -\frac{8}{\pi\nu_o^4}\Bigg[\int_0^{\nu_o}\tau d\tau\int_0^{\cos^{-1}\left(\frac{\nu}{2\nu_o}\right)} d\phi_\tau(-\tau^2\cos^2\phi_\tau + \nu\tau\cos\phi_\tau) \tag{65}$$

$$- \int_0^{\nu/2} d\tau_x\int_0^{\tau_x\frac{2\nu_o}{\nu}\sqrt{1-\left(\frac{\nu}{2\nu_o}\right)^2}} d\tau_y(-\tau_x^2 + \nu\tau_x)\Bigg]\Pi\left(\frac{\nu}{2\nu_o}\right). \tag{66}$$

For the first inner integral we make use of the following identities

$$\int_0^{\cos^{-1} z} d\phi \cos^2\phi = \frac{1}{2} z\sqrt{1-z^2} + \frac{1}{2}\cos^{-1} z, \tag{67}$$

$$\int_0^{\cos^{-1} z} d\phi \cos\phi = \sqrt{1-z^2}, \tag{68}$$

which results in

$$= -\frac{8}{\pi\nu_o^4}\left[\int_0^{\nu_o} d\tau \frac{-\tau^3}{2}\left(\frac{\nu}{2\nu_o}\sqrt{1-\left(\frac{\nu}{2\nu_o}\right)^2} + \cos^{-1}\left(\frac{\nu}{2\nu_o}\right)\right) + \nu\tau^2\sqrt{1-\left(\frac{\nu}{2\nu_o}\right)^2}\right.$$
$$\left.\int_0^{\nu/2} d\tau_x \int_0^{\tau_x \frac{2\nu_o}{\nu}\sqrt{1-\left(\frac{\nu}{2\nu_o}\right)^2}} d\tau_y(-\tau_x^2 + \nu\tau_x)\right]\Pi\left(\frac{\nu}{2\nu_o}\right), \tag{69}$$

$$= -\frac{8}{\pi\nu_o^4}\left[\frac{-\nu_o^4}{8}\left(\frac{\nu}{2\nu_o}\sqrt{1-\left(\frac{\nu}{2\nu_o}\right)^2} + \arccos\left(\frac{\nu}{2\nu_o}\right)\right) + \frac{2\nu_o^4}{3}\frac{\nu}{2\nu_o}\sqrt{1-\left(\frac{\nu}{2\nu_o}\right)}\right.$$
$$\left. - \frac{5\nu^2\nu_o^2}{48}\frac{\nu}{2\nu_o}\sqrt{1-\left(\frac{\nu}{2\nu_o}\right)^2}\right]\Pi\left(\frac{\nu}{2\nu_o}\right), \tag{70}$$

$$= \frac{1}{\pi}\left[\left(\frac{\nu}{2\nu_o}\sqrt{1-\left(\frac{\nu}{2\nu_o}\right)^2} + \arccos\left(\frac{\nu}{2\nu_o}\right)\right) - \frac{16}{3}\frac{\nu}{2\nu_o}\sqrt{1-\left(\frac{\nu}{2\nu_o}\right)}\right.$$
$$\left. + \frac{5\nu^2}{6\nu_o^2}\frac{\nu}{2\nu_o}\sqrt{1-\left(\frac{\nu}{2\nu_o}\right)^2}\right]\Pi\left(\frac{\nu}{2\nu_o}\right), \tag{71}$$

$$= \frac{1}{\pi}\left[\arccos\left(\frac{\nu}{2\nu_o}\right) - \left(\frac{13}{3} - \frac{5\nu^2}{6\nu_o^2}\right)\frac{\nu}{2\nu_o}\sqrt{1-\left(\frac{\nu}{2\nu_o}\right)^2}\right]\Pi\left(\frac{\nu}{2\nu_o}\right), \tag{72}$$

$$= \frac{1}{\pi}\left[\arccos\left(\frac{\nu}{2\nu_o}\right) - \frac{1}{3}\left[13 - 10\left(\frac{\nu}{2\nu_o}\right)^2\right]\frac{\nu}{2\nu_o}\sqrt{1-\left(\frac{\nu}{2\nu_o}\right)^2}\right]\Pi\left(\frac{\nu}{2\nu_o}\right). \tag{73}$$

Next we evaluate the autocorrelation for shifts along the y axis

$$\frac{-2}{\pi\nu_0^4}\left\{\left[\nu_x\,\Pi\left(\frac{\nu}{\nu_o}\right)\right] \star_2^y \left[\nu_x\,\Pi\left(\frac{\nu}{\nu_o}\right)\right]\right\} = \tag{74}$$

$$= \frac{-8}{\pi\nu_o^4}\left[\int_0^{\nu_o} d\tau\,\tau \int_0^{\cos^{-1}\left(\frac{\nu}{2\nu_o}\right)} d\phi_\tau(-\tau^2\sin^2\phi_\tau) - \int_0^{\nu/2} d\tau_x \int_0^{\tau_x\frac{2\nu_o}{\nu}\sqrt{1-\left(\frac{\nu}{2\nu_o}\right)^2}} d\tau_y(-\tau_y^2)\right]\Pi\left(\frac{\nu}{2\nu_o}\right). \tag{75}$$

For the first inner integral we make use of

$$\int_0^{\cos^{-1} z} d\phi \sin^2\phi = -\frac{1}{2} z\sqrt{1-z^2} + \frac{1}{2}\cos^{-1}(z). \tag{76}$$

This results in

$$= \frac{-8}{\pi \nu_o^4}\left[\int_0^{\nu_o} d\tau\, \frac{-\tau^3}{2}\left(\frac{-\nu}{2\nu_o}\sqrt{1-\left(\frac{\nu}{2\nu_o}\right)^2}+\cos^{-1}\left(\frac{\nu}{2a}\right)\right)-\int_0^{\nu/2} d\tau_x \frac{-\tau_x^3}{3}\left(\frac{2\nu_o}{\nu}\sqrt{1-\left(\frac{\nu}{2\nu_o}\right)^2}\right)^3\right]\Pi\left(\frac{\nu}{2\nu_o}\right), \tag{77}$$

$$= \frac{-8}{\pi \nu_o^4}\left[\frac{-\nu_o^4}{8}\left(\frac{-\nu}{2\nu_o}\sqrt{1-\left(\frac{\nu}{2\nu_o}\right)^2}+\cos^{-1}\left(\frac{\nu}{2\nu_o}\right)\right)+\frac{\nu_o^4}{12}\frac{\nu}{2\nu_o}\sqrt{1-\left(\frac{\nu}{2\nu_o}\right)^2}\right]\Pi\left(\frac{\nu}{2\nu_o}\right), \tag{78}$$

$$= \frac{1}{\pi}\left[\cos^{-1}\left(\frac{\nu}{2\nu_o}\right)-\frac{1}{3}\left[5-2\left(\frac{\nu}{2\nu_o}\right)^2\right]\frac{\nu}{2\nu_o}\sqrt{1-\left(\frac{\nu}{2\nu_o}\right)^2}\right]\Pi\left(\frac{\nu}{2\nu_o}\right). \tag{79}$$

Taking the sum of Eqs. 73 and 79 gives the final result

$$A_2(\nu) = \frac{2}{\pi}\left\{\cos^{-1}\left(\frac{\nu}{2\nu_o}\right)-\left[3-2\left(\frac{\nu}{2\nu_o}\right)^2\right]\frac{\nu}{2\nu_o}\sqrt{1-\left(\frac{\nu}{2\nu_o}\right)^2}\right\}\Pi\left(\frac{\nu}{2\nu_o}\right). \tag{80}$$